

中国激光

激光熔覆用 Fe-Cr 合金粉末的紧耦合真空气雾化制备技术

尹燕^{1*}, 董开基¹, 李治恒², 李志慧¹, 柴旭天¹, 张瑞华^{3,4}

¹ 兰州理工大学省部共建有色金属先进加工与再利用国家重点实验室, 甘肃 兰州 730050;

² 新疆大学机械工程学院, 新疆 乌鲁木齐 830047;

³ 中国钢研科技集团有限公司, 北京 100081;

⁴ 阳江市五金刀剪产业技术研究院, 广东 阳江 529533

摘要 采用紧耦合气雾化法制备 Fe-Cr 合金粉末, 分别研究了雾化压力和过热度对粉末粒度分布和表面形貌的影响。结果表明, 在其他工艺参数不变的情况下, 随着雾化压力从 3.0 MPa 增加到 3.4 MPa、3.8 MPa 时, 细粉收得率升高, 粉末中位粒径减小, 气压增大则对液柱的破碎能力增强; 当雾化压力从 3.8 MPa 增加到 4.2 MPa 时, 粗粉收得率提高, 中位粒径增加, 小颗粒粉末团聚或粘结形成大颗粒粉末; 过热度的增加提高了雾化过程的稳定性, 钢液黏度降低、流动性提高, 粉末中位粒径减小, 细粉收得率提高; 过热度增加到 300 °C 时, 液流比增加使液柱破碎不完全, 粉末中位粒径减小。该方法制备的 Fe-Cr 合金粉末的激光熔覆性良好, 熔覆层硬度为 HRC54~HRC57。

关键词 材料; 紧耦合; 气雾化; 粉末; 雾化压力; 过热度

中图分类号 TF123; TF133

文献标志码 A

doi: 10.3788/CJL202148.1402014

1 引言

近年来, 增材制造技术正成为工程制造、材料、光学等学科的研究热点。基于激光与粉末的激光熔化沉积(LMD)和选区激光熔化(SLM)是增材制造技术研发领域较热门的方向^[1], 二者也对金属粉末粒度分布、球形度及氧含量等特性提出了更高的要求^[2-3]。气雾化技术逐渐成为生产金属及合金粉末的主要方法, 有文献指出约 80% 的金属粉末由雾化法制出^[4], 高性能、低成本、批次稳定的粉末制备技术是推动激光熔覆、增材制造等行业产业化、规模化的重要支撑^[5]。气雾化技术制备金属粉末是采用高压高速的雾化气体介质冲击熔融的金属或合金液体, 将其破碎为液滴, 液滴快速凝固为固体粉末颗粒的粉末制备方法。与其他雾化方法相比, 紧耦合气雾化具有粉末粒度细小、球形度高、氧含量低、生产

率高的特点。

粉末颗粒形貌与大小是确定粉末最佳利用率时必须考虑的因素。雾化粉末具有一定的球形度, 这些粉末的流动、堆积、压缩、烧结等性能与形状和大小有关, 研究雾化工艺参数与粉末性能的关系可优化和指导粉末的生产^[6]。Hallén^[7]研究发现影响粉末粒度分布的因素主要是雾化压力、合金成分和雾化喷嘴的结构。金莹等^[8]利用电极感应熔炼气雾化制备 TC4 合金粉末, 随着雾化压力从 3.5 MPa 增加到 7 MPa, 粉末中位粒径先减小后增加, 当雾化压力高于 6 MPa 时, 粒径 < 53 μm 的粉末收得率降低且卫星粉现象明显。数值模拟结果表明^[9], 提高雾化压力与增加雾化气流速度不成比例关系。Özbilen^[10]研究了镁粉的雾化后发现, 在一定雾化压力下, 粗细粉末颗粒形貌不同, 粗颗粒呈长方形和圆形, 细颗粒呈球形。Gao 等^[11]利用双喷嘴感应熔

收稿日期: 2020-11-20; 修回日期: 2021-01-02; 录用日期: 2021-02-18

基金项目: 2018 阳江市重大科技专项(2018002)、阳江市高功率激光应用实验室建设(2018057)、2018 广东省科技计划项目(20180902)

通信作者: *yinyan@lut.cn

炼气雾化 AlSi10Mg 合金,发现雾化压力大于 2.5 MPa 时,细粉收得率增幅减小。过热度是影响粉末雾化效率和粒径分布及雾化过程顺利进行的重要因素,熔体表面张力、黏度、密度等物性影响球形粉的形成^[12]。欧阳鸿武等^[13]研究了过热度对雾化模式和粒度的影响,增加熔体过热度时粉末平均粒径减小,二次破碎模式发生改变,这有助于获得细粉。郑明月^[14]采用气雾化钛合金,熔体过热度增加,则表面张力减小,初始破碎薄膜减薄,粉末中位粒径减小,过热度增加到 350 ℃后,雾化过程稳定性降低,出现的扰动引起中位粒径增加。Ozbilen^[15]通过研究发现随着过热度的增加,粉末变细,不同过热度下粉末形貌不同;吕海波等^[16]研究发现,随着过热度的增加,粉末由不规则的哑铃状、棒状变为球形,且考虑到雾化是否顺利和熔体挥发污染等问题,过热度应确保熔体雾化顺利和尽量减少元素挥发等。目前,国内外对紧耦合真空气雾化粉末全粒度段粉末粒度分布的研究相对较少,鉴于此,本文采用国产紧耦合雾化设备制备 Fe-Cr 合金粉末,重点研究雾化压力和过热度对

全粉末粒度及表面形貌的影响,本研究工作对生产高质量的粉末具有重要的指导意义。

2 试验材料及方法

制粉采用国产真空气雾化设备,该设备主要由熔炼炉、紧耦合雾化器、雾化塔和集粉器组成。试验前将一定纯度的块状原料按比例有序放入熔炼炉,装炉量为 120 kg,合金成分见表 1。采用质量分数为 99.99% 的氩气进行雾化。熔炼前首先抽真空到 5 Pa,然后按一定功率加热,直至完全熔清后采用“双铂铑”热电偶测温;粉末冷却后采用标准筛对粉末进行筛分,采用 LT2200E 激光粒度仪测量粒度分布,采用 JSM-6700 型扫描电子显微镜进行粉末形貌分析。对所制备的 53~105 μm 粒度段粉末进行激光熔覆基础试验,激光器为 Tru Disk2002,同轴送粉,采用质量分数为 99.99% 的氩气保护,采用 HDX-1000 显微硬度计进行硬度测试。熔覆激光功率为 1800 W,离焦量为 15 mm,熔覆速率为 350 mm·min⁻¹,送粉速率为 15 g·min⁻¹,保护气流量为 0.5 L·min⁻¹。

表 1 Fe-Cr 合金化学成分

Table 1 Alloy chemical composition of Fe-Cr

Element	C	Cr	Ni	Mn	Mo	Si	Fe
Mass fraction /%	0.350	15.120	1.100	0.400	0.207	1.503	Balance

3 分析与讨论

3.1 雾化压力对粒度分布及球形度的影响

图 1 为不同雾化压力下 Fe-Cr 合金粉末的累积分布曲线。图 2 为不同雾化压力下的粉末中位粒径。图 3 为不同雾化压力下各粒度段的粉末收得率。从图 1、图 2 和图 3 可以看出,随着雾化压力从 3.0 MPa 增加到 3.4 MPa,累积分布曲线向左移

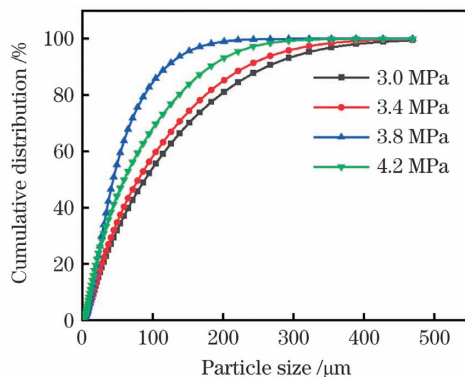


图 1 不同雾化压力下 Fe-Cr 合金粉末累积分布曲线

Fig. 1 Cumulative distribution curves of Fe-Cr alloy powder under different atomizing pressure

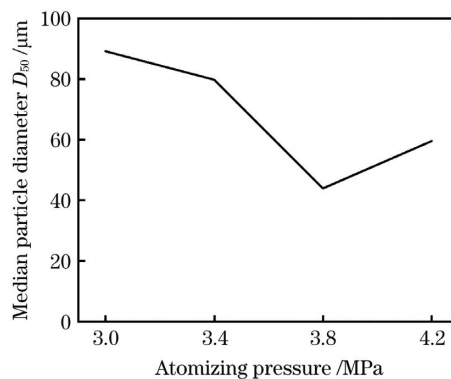


图 2 不同雾化压力下 Fe-Cr 合金粉末的中位粒径

Fig. 2 Median particle size of Fe-Cr alloy powder under different atomizing pressure

动,粉末中位粒径 D_{50} 从 89.226 μm 减小到 79.799 μm,25~53 μm、53~105 μm、105~150 μm 粉末收得率逐渐增加,150 μm 以上的粉末收得率逐渐减小;雾化压力从 3.4 MPa 增加到 3.8 MPa 时,累积分布曲线向左移动,粉末中位粒径 D_{50} 从 79.799 μm 减小到 43.966 μm,25~53 μm、53~105 μm 粉末收得率继续增加,105~150 μm 以及 150 μm 以上的粉末收得率逐渐

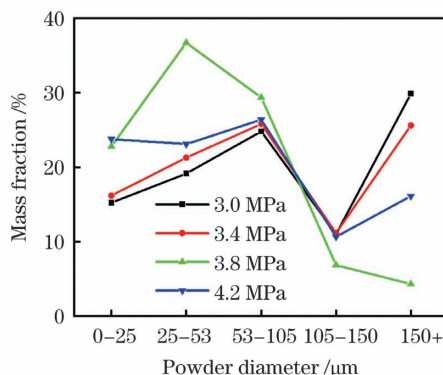


图3 不同雾化压力下Fe-Cr合金粉末各粒度段收得率

Fig. 3 Yield of each grain size segment under different atomizing pressure of Fe-Cr alloy powder

减小；雾化压力继续增加到4.2 MPa时，累积分布曲线右移，粉末中位粒径 D_{50} 由43.966 μm增加到59.601 μm，−25 μm粉末收得率略有增加，25~53 μm、53~105 μm的粉末收得率下降，105~150 μm、150 μm以上粉末收得率上升。

气体雾化过程实际是气体高速运动的动能转化为粉末颗粒的表面能的过程，由(1)式可知，影响气体动能的因素主要是气体速度和气体流量，其中气体速度是影响雾化效率的主要因素。气体动能可表示为

$$J = \frac{1}{2}mv^2, \quad (1)$$

式中： m 是气体流量； v 是气体速度。根据气体动力学原理，增加气体压力同时影响气体速度及导液管末端出口负压。随着雾化压力从3.0 MPa增加到3.4 MPa，雾化气体速度增加，气体动能增加，气体对合金钢液液柱、液膜的冲击力增加，能量转换效率提高，雾化效率提高，单位时间内合金液体更容易破碎为细小的金属液滴^[17-18]，因而−150 μm的粉末收得率不断提高，+150 μm的粉末收得率下降。当雾化压力从3.4 MPa增加到3.8 MPa时，气体流量增幅较气体速度增幅小，能量转换效率不断提高，增加雾化压力使得初次破碎和二次破碎更加剧烈，从而将大颗粒液滴破碎为更加细小的液滴^[19-20]，故−105 μm粉末收得率不断增加，+105 μm粉末收得率不断下降。当压力从3.8 MPa增加到4.2 MPa时，气体压力与速度不成正相关，同时导液管末端出口负压增加引起金属熔体流量增加，导致单位体积内熔体破碎受气体能量影响的增幅减小^[21]，因此出现−105 μm粉末收得率降低、+105 μm粉末收得率显著提高的现象。同时，气体速度增加与金属熔体流量增加引起雾化室气流与液

滴颗粒紊乱程度增加，破碎成的金属小液滴速度大、动能较大，在液滴尚未冷却形成球形粉末之前，液滴之间激烈的碰撞融合形成粒径较大的大颗粒粉末，液滴冷却速度与直径成反比，细小液滴快速凝固粘连在尚未冷凝的金属液滴表面或大颗粒金属液滴包裹小颗粒粉末，因而粉末中位粒径增加。

3.2 过热度对粉末粒度分布及球形度的影响

本文选取雾化压力为3.8 MPa，其他条件不变，过热度分别为150 °C、200 °C、250 °C、300 °C时制备合金粉末。图4为不同过热度下Fe-Cr合金粉末累积分布曲线。图5为不同过热度下Fe-Cr合金粉末中位粒径，图6为不同过热度下Fe-Cr合金粉末各粒度段收得率。

过热度为150 °C时，钢液流至中间包后快速降温，雾化开始后钢液以可见的速度凝结在中间包中形成钢锭。熔体在到达导液管末端时，尚未破碎为金属液滴并缓慢冷却凝固，随着冷却金属不断堆积为“金属瘤”并粘结在导液管末端出口位置，雾化过程中止。

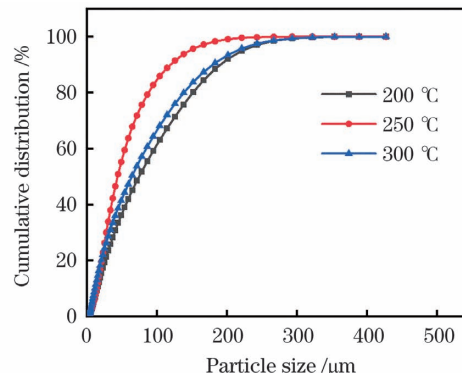


图4 不同过热度下Fe-Cr合金粉末累积分布曲线

Fig. 4 Cumulative distribution curves of Fe-Cr alloy powder under different superheat

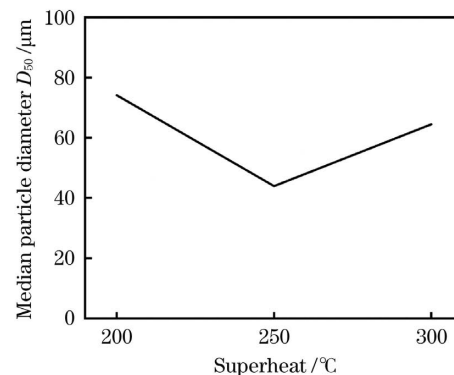


图5 不同过热度下的Fe-Cr合金粉末中位粒径

Fig. 5 Median particle size of Fe-Cr alloy powder under different superheat

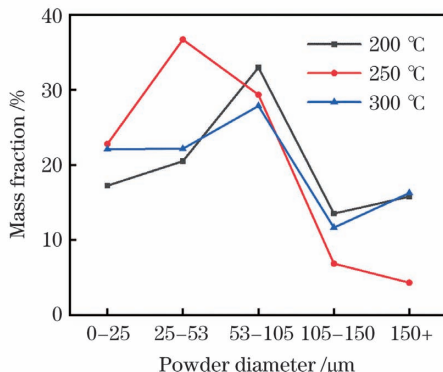


图 6 不同过热度下 Fe-Cr 合金粉末各粒度段收得率

Fig. 6 Yield of each grain size segment under different superheat of Fe-Cr alloy powder

从图 4、图 5 和图 6 可以看出,当金属熔体过热度从 200 °C 增加到 250 °C 时,累积分布曲线向左移动,−25 μm、25~53 μm 粉末收得率增加,53~105 μm、105~150 μm、150 μm 以上粉末收得率下降,金属粉末中位粒径 D_{50} 从 74.857 μm 减小到 43.966 μm;过热度继续增加到 300 °C 时,累积分布曲线右移,金属粉末中位粒径 D_{50} 从 43.966 μm 增加到 64.474 μm,−25 μm、25~53 μm、53~105 μm 粒度段粉末收得率下降,105~150 μm、150 μm 以上粉末收得率上升。

当金属过热度从 200 °C 增加到 250 °C 时,金属熔体的黏度降低、流动性增加,液体体积膨胀,分子间距增大,钢液内能增加^[22]。金属熔体液柱流出导流管后经高速气体冲击破碎,在导流管下方形成倒锥形回流区,液柱被径向回流亚声速气流拉伸为液膜,液膜破碎为液滴,其中部分液滴经过气流二次破

碎形成小颗粒液滴^[23]。过热度过低导致液膜在导流管外部边缘凝固并粘结在导流管上,致使初次破碎不完全。过热度增加使金属液滴表面张力减小,气液界面间的接触角变小,初次破碎形成的薄膜厚度减小,粉末破碎效果得到优化^[24];此外,高速气体直接冲击破碎金属熔体,气体动能向金属熔滴表面能的转化率增加,钢液过热度较高,雾化液体与气流能量交换才能顺利完成^[25~26],所以−53 μm 粉末收得率增加,+53 μm 粉末收得率降低,粉末中位粒径减小。过热度增加到 300 °C 时,熔体破碎成液滴后的冷却凝固时间更长,大小液滴的冷却速度不同,在下落过程中部分小液滴合并成为大液滴,部分液滴在冷却过程中与粉末碰撞或团聚形成棒状或团聚粉末,成为粗粉^[27],故−105 μm 粉末收得率降低,+105 μm 粉末收得率提高,粉末中位粒径增大。过热度过高时炉衬耐火材料发生侵蚀,缩短炉体寿命,同时发生金属元素烧损,所以温度不宜过高。

3.3 粉末形貌特征

图 7 和图 8 分别是相同过热度下不同雾化压力、相同雾化压力下不同过热度条件下的粉末微观组织形貌。表 2 和表 3 分别是不同雾化压力和过热度下的粉末流动性与松装密度。

由表 2 可知,雾化压力增加,粉末流动性先增大后减小,松装密度先增加后减小。从图 7(a)可知,当雾化压力较低时,粉末中大颗粒粉末较多;雾化压力升高,粉末中大颗粒逐渐转变为小颗粒粉末,如图 7(b)和图 7(c)所示;雾化压力升高到 4.2 MPa 时,如图 7(d)所示,粉末中不规则粉末数目增加,小

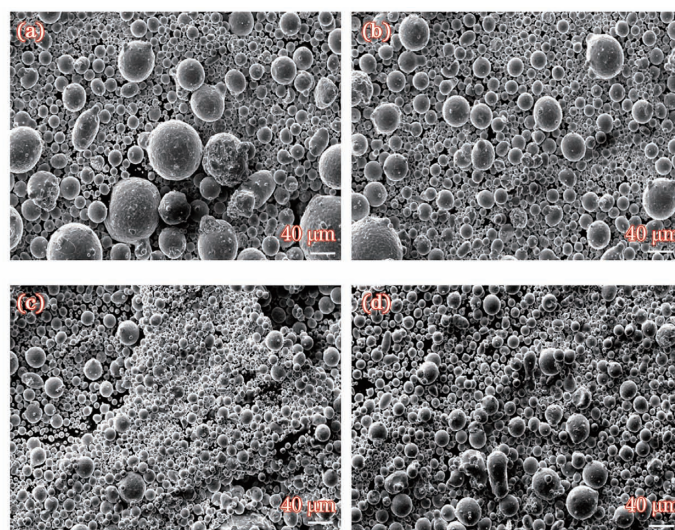


图 7 不同雾化压力下的粉末形貌。(a) 3.0 MPa;(b) 3.4 MPa;(c) 3.8 MPa;(d) 4.2 MPa

Fig. 7 Powder morphologies under different atomizing pressure. (a) 3.0 MPa; (b) 3.4 MPa; (c) 3.8 MPa; (d) 4.2 MPa

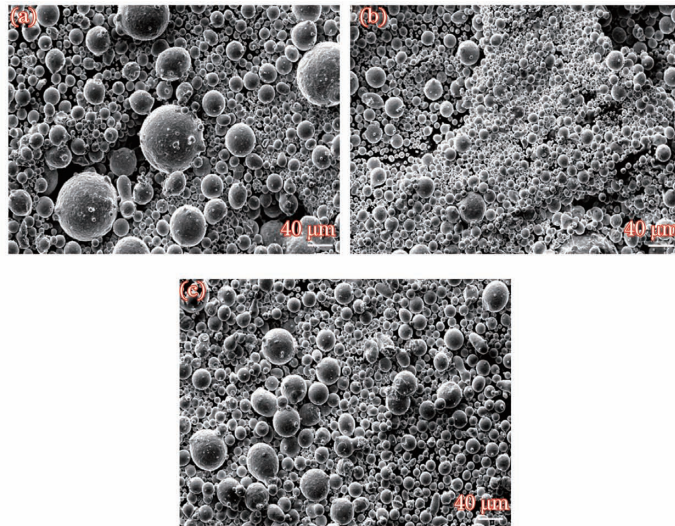


图 8 不同过热度下的粉末形貌。(a) 200 °C; (b) 250 °C; (c) 300 °C

Fig. 8 Powder morphologies under different superheat. (a) 200 °C; (b) 250 °C; (c) 300 °C

颗粒粉末形成团聚状粉末。

由表 3 可知,过热度增加,粉末流动性先增大后减小,松装密度先增大后减小。由图 8(a)和图 8(b)可知,过热度较低时熔融合金液体黏度较大,过热度增加使金属液滴表面张力减小,气液界面间的接触角变小,初次破碎形成的薄膜厚度减小,高速气流对液柱的破碎能力随着黏度的降低而逐渐提高,粉末颗粒由粗粉转变为细颗粒粉末;过热度较高时,熔体破碎成液滴后冷却凝固时间更长,大小液滴在紊流作用下发生碰撞粘结、团聚,同时液体气流比例增加,部分液滴在高速气流破碎作用下破裂为较大颗粒粉末,如图 8(c)所示。

表 2 不同雾化压力下的粉末流动性与松装密度

Table 2 Powder fluidity and bulk density under different atomizing pressure

Atomizing pressure / MPa	Time per 50 g / s	Bulk density / (g · cm ⁻³)
3.0	29.5	4.38
3.4	25.4	4.56
3.8	23.0	4.77
4.2	24.8	4.65

表 3 不同过热度下的粉末流动性与松装密度

Table 3 Powder fluidity and bulk density under different superheat

Superheat / °C	Time per 50 g / s	Bulk density / (g · cm ⁻³)
200	28.4	4.39
250	23.0	4.77
300	23.9	4.68

气雾化制备的粉末球形度可达到 0.85。雾化工艺对粉末形貌影响较大。粉末在重力及表面张力作用下冷却凝固形成球形颗粒,雾化室中存在气流紊流,带动液滴及凝固的粉末颗粒运动,使其碰撞形成不规则粉末,如空心粉、卫星粉、棒状粉等。增加雾化压力可以提高细粉的收得率,同时增加气流、粉末的紊乱度,提高不规则粉末出现的概率,提高金属熔体的过热度。一般而言,降低熔体的黏度及表面张力、增加熔体的流动性,有助于粉末细化^[28],同时延长了液滴的冷却凝固时间。

3.4 合金粉末激光熔覆

所制备的合金粉末主要针对常用的 3Cr13 不锈钢厨刀刀刃进行改性,提高其耐磨性,故采用 3Cr13 不锈钢刀条为基体,进行激光熔覆试验。图 9 为优化工艺后激光熔覆试样的宏观形貌,图 10 为刀刃截面宏观形貌。从图 9 可以看出,熔覆层光滑连续,成形良好,表面呈金属光泽。从图 10 可知,熔覆层截面形成了三个典型的区域,即熔覆层、过渡区和基体。熔覆层与基体结合良好,且熔覆层内部组织致密,没有裂纹、气孔和夹杂等缺陷。X 射线检测后熔覆层无气孔、裂纹。平行于熔覆层长度方向取样,磨平熔覆层顶部以测试洛氏硬度。测试 5 个位置得到的硬度值分别为 HRC55.2、HRC56.3、HRC56.8、



图 9 熔覆层宏观形貌

Fig. 9 Macro morphology of cladding layer

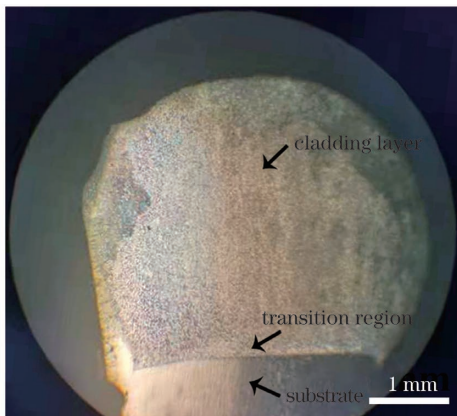


图 10 刀刃截面宏观形貌

Fig. 10 Macro morphology of blade section

HRC57.3、HRC54.9。

综上可见,采用紧耦合真空气雾化法制备 Fe-Cr 合金粉末时,制备过程中的高真空度可有效降低合金粉末中的氧含量;高的球形度及合适的粒径范围是良好的同轴送粉激光熔覆性基础;合金粉末中 Mn、Si 元素的调控对合金粉末激光熔覆成形性具有良好作用;Ni 元素促进熔覆层基体奥氏体化,可使基体韧性增加。熔覆层硬度高于基体 3Cr13 的 HRC40。

4 结 论

采用紧耦合真空气雾化制备激光熔覆用 Fe-Cr 合金粉末,研究了雾化工艺对全粒度段粉末粒度分布及球形度的影响,并得到以下结论:1)紧耦合制备 Fe-Cr 合金粉末,相同过热度条件下,随着雾化气体压力的增加,气体对液柱的破碎能力增强,使得粗粉转化为细粉,粉末中位粒径减小,<105 μm 粉末收得率提高,继续增加雾化压力到 4.2 MPa,液流比增加,细粉收得率下降;2)雾化压力不变时,熔体过热度影响雾化过程,提高熔体的过热度可降低熔体黏度、提高流动性,粉末中位粒径减小,细粉收得率增加;3)熔体过热度过高时,大颗粒粉末表面粘附大量卫星粉和细粉块,粉末中位粒径增加,流动性降低;4)所制备的 Fe-Cr 合金粉末同轴送粉的激光熔覆成形良好,熔覆层硬度为 HRC54~HRC57,高于基体 3Cr13 不锈钢。

参 考 文 献

- [1] Gu D D, Zhang H M, Chen H Y, et al. Laser additive manufacturing of high-performance metallic aerospace components[J]. Chinese Journal of Lasers, 2020, 47(5): 0500002.

顾冬冬,张红梅,陈洪宇,等.航空航天高性能金属材料构件激光增材制造[J].中国激光,2020,47(5): 0500002.

- [2] Hu Z H, Song C H, Liu L Q, et al. Research progress of selective laser melting of nitinol[J]. Chinese Journal of Lasers, 2020, 47(12): 1202005. 胡泽华,宋长辉,刘林青,等.镍钛合金激光选区熔化成形技术研究进展[J].中国激光,2020,47(12): 1202005.
- [3] Hu Y, Liu S S, Cheng X, et al. Finite element simulation on bending properties of TA2/TA15 gradient material by laser direct deposition[J]. Chinese Journal of Lasers, 2020, 47(12): 1202006. 胡悦,刘莎莎,程序,等.激光直接沉积 TA2/TA15 梯度材料弯曲性能的有限元模拟[J].中国激光,2020,47(12): 1202006.
- [4] Dowson A G. Atomization dominates powder production[J]. Metal Powder Report, 1999, 54(1): 15-17.
- [5] Wang B Y, Lu L, Wu W H, et al. The research progress of powder preparation technology by gas atomization[J]. Powder Metallurgy Industry, 2019, 29(5): 74-80. 王博亚,卢林,吴文恒,等.气雾化制粉技术研究进展[J].粉末冶金工业,2019,29(5): 74-80.
- [6] Amada S, Ohyagi T, Haruyama M. Evaluation of splat profile for droplet impingement[J]. Surface and Coatings Technology, 1999, 115(2/3): 184-192.
- [7] Hallen H. A study of size distribution and microstructure of gas atomized powder[J]. Metal Powder Report, 1997, 52(4): 46-47.
- [8] Jin Y, Liu P, Shi J G, et al. Effects of gas-atomized pressure on morphology and properties of TC4 powder prepared by electrode-induced gas atomization[J]. Materials Science and Engineering of Powder Metallurgy, 2018, 23(3): 312-317. 金莹,刘平,史金光,等.雾化压力对电极感应熔炼气雾化 TC4 粉末形貌与性能的影响[J].粉末冶金材料科学与工程,2018,23(3): 312-317.
- [9] Aydin O, Unal R. Experimental and numerical modeling of the gas atomization nozzle for gas flow behavior[J]. Computers & Fluids, 2011, 42(1): 37-43.
- [10] Özbilen S. Influence of atomizing gas pressure on particle shape of Al and Mg powders[J]. Powder Technology, 1999, 102(2): 109-119.
- [11] Gao C F, Xiao Z Y, Zou H P, et al. Characterization of spherical Al₁Si₁₀Mg powder produced by double-nozzle gas atomization using different parameters[J]. Transactions of Nonferrous Metals Society of China, 2019, 29(2): 374-384.

- [12] Strauss J T, Miller S A. Effect of melt superheat on close coupled gas atomized powder characteristics[J]. Metal Powder Report, 1997, 52(4): 46.
- [13] Ouyang H W, Chen X, Yu W T, et al. Effect of melt superheat on powder particle size in close-coupled gas atomization[J]. Chinese Journal of Rare Metals, 2006, 30(S1): 84-88.
欧阳鸿武, 陈欣, 余文焘, 等. 紧耦合气雾化制粉中熔体过热度对雾化模式和粉末粒度的影响[J]. 稀有金属, 2006, 30(S1): 84-88.
- [14] Zheng M Y. Gas atomization technology research of titanium alloy powders for additive manufacturing [D]. Beijing: University of Science and Technology Beijing, 2019.
郑明月. 气雾化法制备增材制造用钛合金粉末研究[D]. 北京: 北京科技大学, 2019.
- [15] Ozbilin S. Influence of superheat temperature on particle size and shape of gas atomized copper powders: S. Özbilen et al, (Imperial Coll, London, UK Powder Metallurgy, Vol 34, No 1 1991, 53-61 [J]. Metal Powder Report, 1992, 47(1): 49.
- [16] Lu H B, Mu Y F. Influences of melt superheat on atomization procedure[J]. Journal of Central South University of Technology, 1997(2): 149-151.
吕海波, 母育锋. 熔体过热度对雾化过程的影响[J]. 中南工业大学学报, 1997(2): 149-151.
- [17] Ünal A. Liquid break-up in gas atomization of fine aluminum powders[J]. Metallurgical Transactions B, 1989, 20(1): 61-69.
- [18] Ouyang H W, Huang B Y, Chen X, et al. Filming mechanism of high-pressure gas atomization in state of 'opened' wake [J]. The Chinese Journal of Nonferrous Metals, 2005, 15(7): 1000-1005.
欧阳鸿武, 黄伯云, 陈欣, 等. 开涡状况下紧耦合气雾化的成膜机理[J]. 中国有色金属学报, 2005, 15(7): 1000-1005.
- [19] Ouyang H W, Chen X, Yu W T, et al. Preparation of amorphous powders of Al-based alloy by close-coupled gas atomization [J]. Rare Metal Materials and Engineering, 2006, 35(6): 866-870.
欧阳鸿武, 陈欣, 余文焘, 等. 紧耦合气雾化制备Al基合金非晶粉末的研究[J]. 稀有金属材料与工程, 2006, 35(6): 866-870.
- [20] Ouyang H W, Wang Q, Liu Z M. Numerical study on abrupt change of flow field in close-coupled gas atomization[J]. Materials Science and Engineering of Powder Metallurgy, 2010, 15(2): 96-101.
欧阳鸿武, 王琼, 刘卓民. 紧耦合气雾化流场结构突变过程的数值模拟[J]. 粉末冶金材料科学与工程, 2010, 15(2): 96-101.
- [21] Wu W H, Wu K Q, Xiao Y F, et al. Effect of atomization pressure on the properties of 316L stainless steel powders used in 3D printing [J]. Powder Metallurgy Technology, 2017, 35 (2): 83-88.
吴文恒, 吴凯琦, 肖逸凡, 等. 气雾化压力对3D打印用316L不锈钢粉末性能的影响[J]. 粉末冶金技术, 2017, 35(2): 83-88.
- [22] Xu T H, Zhao M Q, Di X B, et al. Influences of superheat of alloy on the properties of free-lead solder power of Sn-Ag-Cu system [J]. Materials Review, 2005, 19(4): 128-130.
许天旱, 赵麦群, 邸小波, 等. 过热度对无铅焊锡雾化粉末特性的影响[J]. 材料导报, 2005, 19(4): 128-130.
- [23] Li Q Q. The principle of powder production by the close-coupled gas atomization[J]. Powder Metallurgy Industry, 1999, 9(5): 3-17.
李清泉. 紧密耦合气体雾化制粉原理[J]. 粉末冶金工业, 1999, 9(5): 3-17.
- [24] Zheng M Y, Zhang S M, Hu Q, et al. Microstructural characterisation of CuAgZr powder particles produced by argon gas atomisation [J]. Powder Metallurgy, 2018, 61(3): 231-240.
- [25] Ting J, Anderson I E. A computational fluid dynamics (CFD) investigation of the wake closure phenomenon[J]. Materials Science and Engineering: A, 2004, 379(1/2): 264-276.
- [26] Ting J, Peretti M W, Eisen W B. The effect of wake-closure phenomenon on gas atomization performance[J]. Materials Science and Engineering: A, 2002, 326(1): 110-121.
- [27] Ünal A. Effect of processing variables on particle size in gas atomization of rapidly solidified aluminium powders [J]. Materials Science and Technology, 1987, 3(12): 1029-1039.
- [28] Özbilen S, Ünal A, Sheppard T. Influence of liquid metal properties on particle size of inert gas atomized powders [J]. Powder Metallurgy, 1996, 39 (1): 44-52.

Preparation of Fe-Cr Alloy Powder by Close-Coupled Vacuum Induction Melting Gas Atomization for Laser Cladding

Yin Yan^{1*}, Dong Kaiji¹, Li Zhiheng², Li Zhihui¹, Chai Xutian¹, Zhang Ruihua^{3,4}

¹ State Key Laboratory of Advanced Processing and Recycling of Nonferrous Metals, Lanzhou University of Technology, Lanzhou, Gansu 730050, China;

² School of Mechanical Engineering, Xinjiang University, Urumqi, Xinjiang 830047, China;

³ Central Iron and Steel Research Institute, Beijing 100081, China;

⁴ Yangjiang Hardware Knife Cut Industrial Technology Research Institute, Yangjiang, Guangdong 529533, China

Abstract

Objective Recently, with the continuous development of laser additive manufacturing, the demand for metal powder is increasing. Vacuum induction melting gas atomization is a new technology that combines vacuum induction smelting technology and inert gas atomization technology. Systems based on this technology exhibit low oxygen content, good sphericity, and high yield. Therefore, this technology is suitable for preparing high-performance powder materials with various particle size requirements. The atomizer is instrumental to vacuum induction melting gas atomization. Compared with the free-fall atomizer, the close-coupled atomizer has a compact structure with a guide pipe that allows metal to melt and flow out. Consequently, a small flight distance and a high atomization efficiency are achieved. Currently, research on close-coupled vacuum induction melting gas atomization mainly focuses on the study of the particle size distribution and properties of a certain section of the particle size, while research on the particle size distribution and properties of the entire section of the particle size is relatively few. Moreover, there is a lack of theoretical guidance for powder production. In this study, the effects of atomizing pressure and superheat on the size distribution and properties of the powder particles in the process of close-coupled vacuum induction melting gas atomization were studied. Further, reasons for the change in the powder particle size and properties were analyzed. Based on different powder size requirements of various industries, this study will play a guiding role in powder preparation.

Methods Herein, the vacuum degree reached 5 Pa, and the argon gas with 99.99% purity was used for atomization. The single variable control method was used to study the effects of atomizing pressure and superheat on the particle size distribution and surface morphology, respectively, during the close-coupled gas atomizing process of Fe-Cr alloy powder. After cooling, 500-g powder was randomly weighed and screened using a standard vibrating screen. The screen mesh was selected as 100 mesh (150 μm), 150 mesh (105 μm), 270 mesh (53 μm), and 500 mesh (25 μm). Then, an electronic scale was used to weigh the mass of each particle size section. A small amount of powder was randomly selected to measure the cumulative distribution using a laser particle size analyzer. The powder morphology was observed using a scanning electron microscope. The bulk density and fluidity testers were used to measure the bulk density and fluidity. Laser cladding technology was used to clad the powder onto 3Cr13 stainless steel, and the macromorphology and rockwell hardness of the laser cladding layer were studied.

Results and Discussions Results show that when other atomization parameters are the same, the cumulative distribution curves of the powder move to the left and then move to the right when the atomizing pressure is further increased to 4.2 MPa. The median particle size of the corresponding powder first decreases and then increases. The yield rate of the powder with a size of $-105 \mu\text{m}$ first increases and then decreases (Fig. 3). Both the powder fluidity and bulk density first increase and then decrease (Table 2). The stability of the atomization process is improved by increasing superheat. At 150 $^{\circ}\text{C}$ superheat, the metal shows a “metal tumor” at the end of the tube, which halts the atomization process. When the superheat is increased to 200 $^{\circ}\text{C}$ and 250 $^{\circ}\text{C}$, the liquid steel viscosity decreases, the fluidity increases, and the cumulative distribution curves of the powder move to the left. When the superheat is further increased to 300 $^{\circ}\text{C}$, the cumulative distribution curves of the powder move to the right. The median particle size of the corresponding powder first decreases and then increases. Moreover, the yield of the fine powder first increases and then decreases (Fig. 6). Both the powder fluidity and bulk density first increase and then decrease (Table 3).

Conclusions When the atomizing pressure and gas velocity are increased, the breakability of the alloy liquid column is improved. When the atomizing pressure is increased to 4.2 MPa, the gas pressure is increased significantly more compared with the gas velocity. Moreover, increasing the gas pressure results in an increase in the negative pressure at the end outlet of the liquid guide tube, which increases the metal melt flow. The broken melt is affected by a decrease in the gas energy per unit volume. The increased degree of gas flow disorder causes the collision and fusion of droplets, thus forming a coarse powder. Thus, the median particle size increases. When the superheat is increased, the surface tension in the metal droplets is decreased and the contact angle between the gas-liquid interface is decreased. Consequently, the thickness of the film formed by the initial crushing is decreased, optimizing the crushing effect. When the superheat is increased to 300 °C, the cooling and solidification times of the metal melt and broken into droplets is longer. The cooling speed differs for droplets with different sizes. During the falling process, some small droplets combine into large ones and some droplets collide or agglomerate with the powder in the cooling process to form rods or agglomerate into a coarse powder. Therefore, the median particle size of the powder increases. The laser cladding layer of the alloy powder prepared using the vacuum induction melting gas atomization technology shows good properties, and the hardness of the cladding layer is HRC54–HRC57.

Key words materials; close-coupling; gas atomization; powder; atomizing pressure; superheat

OCIS codes 160.3900, 310.3840, 350.3850